Discrete element modeling and parameter calibration of safflower biomechanical properties

Zhenguo Zhang[1,2*], Chao Zeng[1,2], Zhenyu Xing[1,2], Peng Xu[1,2], Quanfeng Guo[1,2], Ruimeng Shi[1,2], Yunze Wang[1,2]

(1. *College of Mechanical and Electrical Engineering, Xinjiang Agricultural University, Urumqi 830052, China*;
2. *Key Laboratory of Xinjiang Intelligent Agricultural Equipment, Xinjiang Agricultural University, Urumqi 830052, China*)

Abstract: Understanding the biomechanical properties of safflowers is essential for appropriately designing harvesting machinery and optimizing the harvesting process. Safflower is a flexible crop that lacks a basis for relevant simulation parameters, which causes difficulties in designing harvesting machinery. In this study, a calibration method for safflowers was proposed. First, a discrete element model was established by measuring the intrinsic parameters of a safflower, such as its geometric parameters, density, Poisson's ratio, and modulus of elasticity. Second, the contact and bonding parameters were calibrated using a combination of physical and simulation tests. In the contact parameter tests, the Hertz-Mindlin (no-slip) model was implemented for the stacking angle tests conducted regarding the safflower filament. A regular two-level factorial design was used to determine the important factors and perform the steepest climb test. Moreover, the Box-Behnken design was adopted to obtain the optimal contact parameters. In the bonding parameter tests, the Hertz-Mindlin model with bonding contact was applied for the safflower shear simulation tests; moreover, the optimum bonding parameters were obtained through the central composite design test. The results demonstrated that the relative errors between the simulated and measured stacking angles and maximum shear were 3.19% and 5.29%, respectively. As a result, the safflower simulation parameters were accurately calibrated, providing a reference for appropriately setting the simulation parameters and designing key mechanical components.

Keywords: safflower, DEM, parameter calibration, shear test, biomechanical properties
DOI: 10.25165/j.ijabe.20241702.8857

Citation: Zhang Z G, Zeng C, Xing Z Y, Xu P, Guo Q F, Shi R M, et al. Discrete element modeling and parameter calibration of safflower biomechanical properties. Int J Agric & Biol Eng, 2024; 17(2): 37–46.

1 Introduction

Safflower (*Carthamus tinctorius L.*) is a commercial cash crop planted worldwide and has a wide range of applications, including food, medicinal herbs, textile dyeing, etc[1-3]. Xinjiang, China, owing to its unique geographical and climatic conditions, is a rich safflower resource with a planting area of nearly 40 000 hm^2[4-6]. Currently, progress has been made in the research on safflower harvesting machinery, especially regarding end actuators[7,8]. Because of the soft and complex morphology of safflower filaments, their biomechanical properties are difficult to analyze using Newtonian mechanics tests, which results in the lack of a basis for setting the relevant actuator parameters for safflower harvesting[9]. A possible solution to this problem is using discrete-element simulations to study the microscopic mechanisms of safflowers. The discrete element method (DEM) has significant advantages when studying the biomechanical properties of crops and their mechanical interaction[10-12]. Therefore, establishing a discrete element model of safflower can expedite the in-depth exploration of its biomechanical properties and provide a theoretical basis for designing corresponding machinery.

The calibration research for contact modeling and parameters is an important part of agricultural materials simulation studies[13,14]. The reliability of discrete element calibration depends on the simulation model and corresponding parameters[15,16]. Discrete element models can be classified into two types, namely, rigid and flexible models[17]. DEM based on a rigid model has been more commonly applied to the simulation of crop properties and optimization of harvesting device parameters[18-20]. Chen et al.[21] proposed a discrete element model for alfalfa stalks and applied the Hertz-Mindlin model with a bonding contact model to characterize their biomechanical properties. Zhou et al.[22] presented a discrete element model for banana stalks by studying the shear, tensile, compression, and bending of banana various bunch stems. Their results showed that the internode position and water content of the banana stalks could significantly affect the mechanical properties of banana stalks. Li et al.[23] established a discrete element model of corncob. Accordingly, they used the maximum shear force as the test index to explore the interaction between corn stover and implements, which aids other crop-implement interaction studies.

Received date: 2024-02-06 **Accepted date:** 2024-03-10
Biographies: Chao Zeng, MS, research interest: characteristic crops quality improvement and efficiency technology and intelligent equipment, Email: chaozeng5054@163.com; **Zhenyu Xing**, Master, research interest: characteristic crops quality improvement and efficiency technology and intelligent equipment, Email: xingzhenyu151621@163.com; **Peng Xu**, MS, research interest: characteristic crops quality improvement and efficiency technology and intelligent equipment, Email: xupeng9018@163.com; **Quanfeng Guo**, MS, research interest: characteristic crops quality improvement and efficiency technology and intelligent equipment, Email: guoquanfengnl@163.com; **Ruimeng Shi**, MS, research interest: characteristic crops quality improvement and efficiency technology and intelligent equipment, Email: 19199276782@163.com; **Yunze Wang**, MS, research interest: characteristic crops quality improvement and efficiency technology and intelligent equipment, Email: Wangyunze_531@163.com.

***Corresponding author: Zhenguo Zhang**, Associate Professor, research interest: characteristic crops quality improvement and efficiency technology and intelligent equipment. College of Mechanical and Electrical Engineering, Xinjiang Agricultural University, No.311, Nongda East Road, Urumqi 830052, China. Tel: +86-15099092586, Email: zhangzhenguo@xjau.edu.cn.

Zhang et al.[24] established a discrete element model of panax pseudo-ginseng stalks. The contact and bonding parameters of the model were verified via stacking angle and shear tests, respectively, which provided simulation optimization references to design a reciprocating cutter for panax pseudo-ginseng rice plant-killing device. Most of the aforementioned studies modeled rigid stalk crops. However, safflower is a flexible floral crop. The morphology of safflower stems is more complex than that of stalk crops. Meanwhile, there are fewer DEM reports related to safflower and a lack of references to similar materials. The method of parameter calibration has important applications for obtaining material parameters. Therefore, the parameter calibration of safflower is crucial for conducting safflower in simulation studies.

In this study, a discrete element model of safflower was established so that the intrinsic parameters of safflower material can be determined. The Hertz-Mindlin (no-slip) contact model was first selected for the stacking angle test. The optimum contact parameters were obtained using the Box-Behnken design. Accordingly, the Hertz-Mindlin model with bonding contact was applied for the safflower shear simulation tests, and the optimum bonding parameters were obtained via the central composite design test. Using the stacking angle and the maximum shear as the response indices, the obtained simulation parameters were verified by conducting further simulations and physical tests. The results provide the basic parameters for investigating the biomechanical properties of safflower and simulating the safflower harvesting process, as well as help in the calibration of corresponding parameters for similar crops.

2 Materials and methods

2.1 Test materials

Yunhong No.6, a safflower type commonly cultivated in China, was used as the test material. It was sampled from the Yunguang safflower planting base in the Ili Kazakh Autonomous Prefecture in July 2023. The structure of safflower consists mainly of filaments, a necking, and a fruit ball[25], where necking is defined as the position of interaction with the shear mechanism, as shown in Figure 1. Three-dimensional parameters of safflower were measured using the Vernier scale (DL92150P, range 0-150 mm, accuracy 0.01 mm, developed by Deli Group Co., Ltd.), namely, the filament width w, fruit ball height h, necking diameter D_1 and fruit ball diameter D_2. The measurement results are listed in Table 1, which provides a basis for constructing a discrete elemental model of safflower.

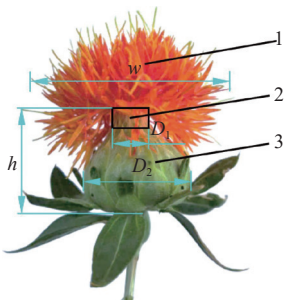

Figure 1 Composition of safflower and key geometric parameters

Table 1 Main feature parameters of safflower

Parameters	Mean value/mm	Coefficient of variation/%
w	48.29	1.56
h	21.60	9.29
D_1	4.85	16.46
D_2	25.15	16.46

2.1.1 Safflower intrinsic parameters

The intrinsic safflower parameters were its density, Poisson's ratio, and shear modulus. The average density of safflower (wet basis) was 400 kg/m^3, measured by a measuring cylinder (range 0-500 ml, accuracy 5 mL, developed by Fuzhou North Glass Experimental Instrument Co., Ltd.) and electronic scale (I-2000, range 0-500 g, accuracy 0.01 g, developed by Deqing Bayjie Electric Appliance Co., Ltd.). The Poisson's ratio and shear modulus were determined by uniaxial compression tests using a texture analyzer (TMS-Pro, range 250 N, accuracy 0.01 N, FTC Co., Ltd., USA). The compression speed was set to 5 mm/min, loading displacement was set to 4 mm, and changes in necking height and diameter were measured before and after the uniaxial compression test. The Poisson's ratio and shear modulus were calculated using Equations (1) and (2)[26].

$$E = \frac{F/A}{\Delta L/L} \tag{1}$$

$$G = \frac{E}{2(1+\mu)} \tag{2}$$

where, E is the modulus of elasticity, Pa; F is the compression force, N; A is the compression area, m^2; L is the effective length, m; ΔL is the change in effective length, m; G is the shear modulus, Pa; and μ is the Poisson's ratio.

The test was repeated ten times. Finally, the Poisson's ratio and shear modulus were calculated as 0.25 and 1 MPa, respectively.

2.1.2 Safflower contact parameters

Safflower contact parameters were determined using filament stacking angle tests. The test was performed on an electro-mechanical universal testing machine (developed by Shenzhen Rigel Instrument Co., Ltd.), using a steel cylinder (50 mm in diameter and 300 mm in height) by pouring up to 250 mL of the safflower filaments. The electro-mechanical universal testing machine controlled the cylinder to rise slowly at a speed of 0.1 m/s. The safflower filaments flowed downward by gravity, resulting in a filament stack. A high-definition camera was used to take a front-view image of the safflower filament stack (Figure 2a). To reduce the measurement error, the filament stacking angle was measured using MATLAB software[27]. First, the left half of the image was intercepted from the initial image (Figure 2b) and binarized (Figure 2c). Next, the image boundary points were extracted to obtain the boundary curves, and a linear equation was fitted (Figure 2d). Accordingly, the following equation was obtained y_c= 0.632x–1.046. The slope of the equation for both the horizontal and filament slopes was 0.632, and the angle of accumulation was measured as 32.29°. After five repetitions, the average stacking angle was measured as 30.80°.

2.1.3 Safflower bonding parameters

Safflower necking denotes the formation of an overflow of filament clusters, which reflects the main biomechanical characteristics of safflower. The safflower bonding parameters were obtained by performing necking shear tests using a texture analyzer. The texture analyzer was set up with an initial force of 50 N, speed of 20 mm/min, return speed of 20 mm/min, and return distance of 30 mm, as shown in Figure 3. The maximum shear force was 58.27 N and the average shear force was 43.36 N for the ten groups of samples.

2.2 Safflower discrete element model

2.2.1 Selection of contact model

According to the practical requirements of the filament stacking angle test, the filament model was incompressible and non-viscous.

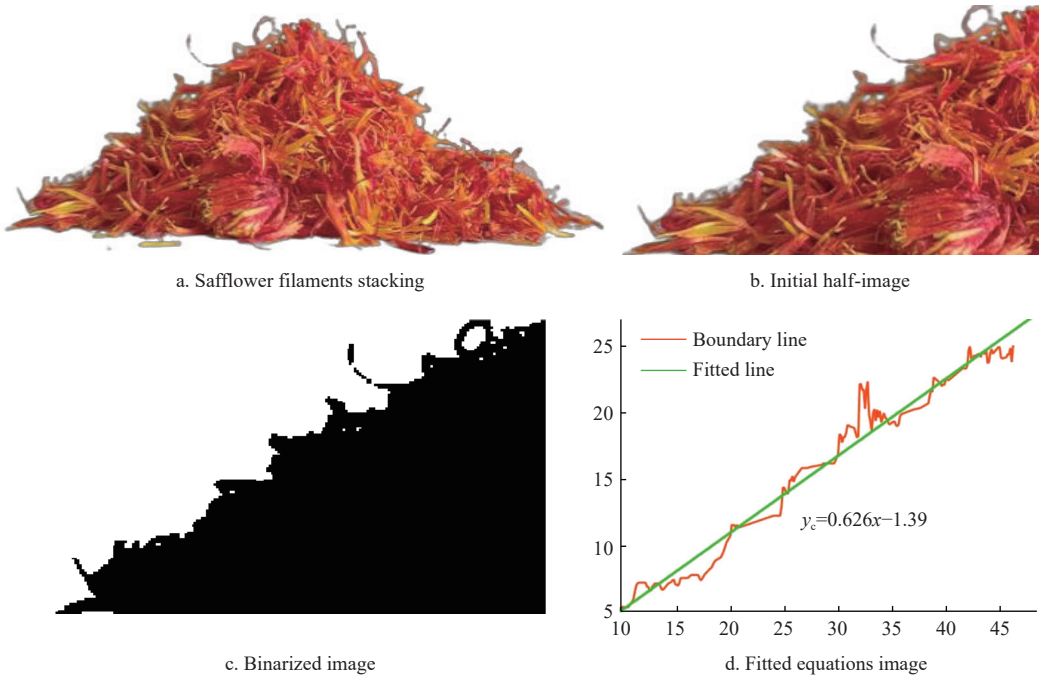

a. Safflower filaments stacking b. Initial half-image

c. Binarized image d. Fitted equations image

Figure 2 Physical stacking angle test of safflower filaments

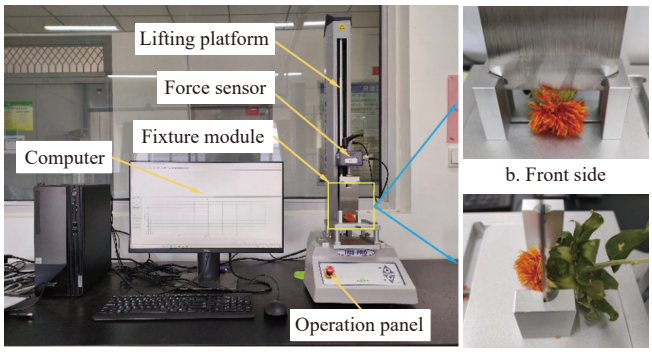

a. Composition of the texture analyzer b. Front side c. Lateral side

Figure 3 Safflower shear tests for texture analyzer

Therefore, the Hertz-Mindlin (no-slip) model was chosen as the contact model. Based on the biomechanical properties of safflower, the shear test implemented the Hertz-Mindlin model with bonding contact to describe the particle-particle interactions within safflower. In the Hertz-Mindlin model with bonding[28], the force between two particles is described by proper bonding (Figure 4).

The forces and torques acting on the particle are defined in Equations (3)-(6)[29].

$$\delta F_n = v_n k_b^n A \delta_t \tag{3}$$

$$\delta F_t = -v_t k_b^s A \delta_t \tag{4}$$

$$\delta M_n = -\omega_n k_b^s J \delta_t \tag{5}$$

$$\delta M_s = -\omega_t k_b^n J \delta_t / 2 \tag{6}$$

where, A is the contact area, m^2; k_b^n and k_b^s are the normal and shear stiffness per unit area, N/m^3; δ_t is the time step, s; v_n and v_t are the normal and shear velocities of the particles, m/s; respectively, ω_n and ω_t are the normal and shear angular velocities of the particles, rad/s, respectively; δM_n and δM_t represent the torque of the bond in the normal and shear directions, N·m, respectively; δF_n and δF_t are the normal and shear bond forces of the bonding bond, N, respectively; and J is the particle moment of inertia, kg·m^2.

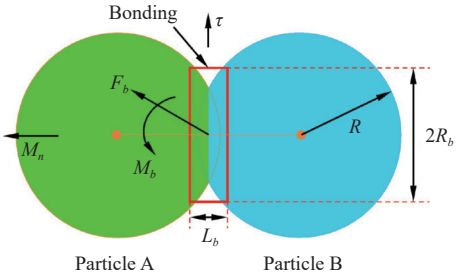

Note: F_b is the combined force due to particle A acting on particle B, N; M_n and M_b are the normal and shear moments, N·m, respectively; L_b is the bonded portion of particles A and B, m; R_b is the radius of the bonding bond, mm; R is the radius of the particle, mm; and τ is the shear critical stress, N.

Figure 4 Hertz-Mindlin model with bonding

Both the shear and normal forces between the particles act on the bonds. When these forces exceed a predetermined value, the bond breaks, under the conditions stated in Equations (7) and (8). Thus, the broken state of safflower can be modeled from the state of bonding[30,31].

$$\sigma_{max} < \frac{-F_n}{A} + \frac{2M_t}{J} R_b \tag{7}$$

$$\tau_{max} < \frac{-F_t}{A} + \frac{M_n}{J} R_b \tag{8}$$

where, σ_{max} and τ_{max} are the normal and shear critical stresses, N, respectively.

2.2.2 simulation model of filaments

Establishing an accurate 3D model of the filaments is the basis for verifying the contact parameters. Safflower is significantly different from traditional root and stem crops, and the irregular shape and soft texture of the filaments make it difficult to obtain an accurate outline its shape. To improve the simulation accuracy, filament models were established based on the natural growth state and actual harvesting process. The damage to individual filaments was categorized into three typical filament morphologies: complete filaments (Figure 5a), damaged filaments (Figure 5b), and mutilated filaments (Figure 5c). Discrete models of the filaments with the

same morphology were built using EDEM2020 software, as shown in Figure 5.

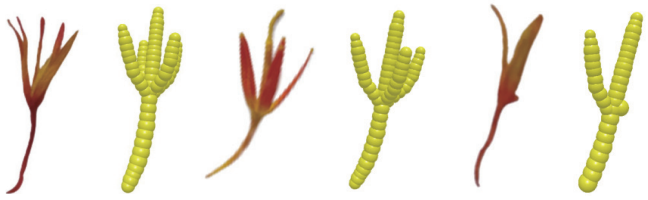

a. Complete filament b. Damaged filament c. Mutilated filament

Figure 5 Filament models.

The simulation test established the same cylinder as the physical test, using steel as the material. The steel material parameters were directly extracted from the material library of the EDEM software, namely, steel Poisson's ratio, density, and shear modulus were 0.3, 7950 kg/m^3 and 7.94×10^4 MPa, respectively. The contact parameters of the safflower filament refer to the agricultural and floral material simulation parameters; the range of values is listed in Table 2.

The high-level combinations listed in Table 2 are used to test the contact parameters. The top of the cylinder was added to the virtual surface and set as the particle factory. The filament particles were dynamically generated under speed, total amount, and time conditions of 0.5 m/s, 0.2 kg, and 0.65 s, respectively. After filament particle generation was completed and stabilized, the cylinder was lifted upward at a speed of 0.1 m/s. The particles flowed from the bottom of the cylinder and formed a stable pile after settling (Figure 6a). The filament simulation stack angle was measured using the same method as that used in the physical tests (Figures 6b-6d). Finally, the corresponding simulation fitting equation was obtained, y_{cs}=0.723x+1.331. The slope of the equation for both the horizontal and filament slopes was 0.723, and the simulation stacking angle of the high-level combinations was 35.87°.

Table 2 Range of values for contact parameters

Symbol	Simulation Parameter	Low level (–1)	High level (+1)
X_1	Impact recovery coefficient of safflower-safflower	0.05	0.25
X_2	Rolling friction coefficient of safflower-safflower	0.15	0.60
X_3	Static friction coefficient of safflower-safflower	0.15	0.60
X_4	Impact recovery coefficient of safflower-steel	0.10	0.60
X_5	Rolling friction coefficient of safflower-steel	0.30	0.60
X_6	Static friction coefficient of safflower-steel	0.10	0.40

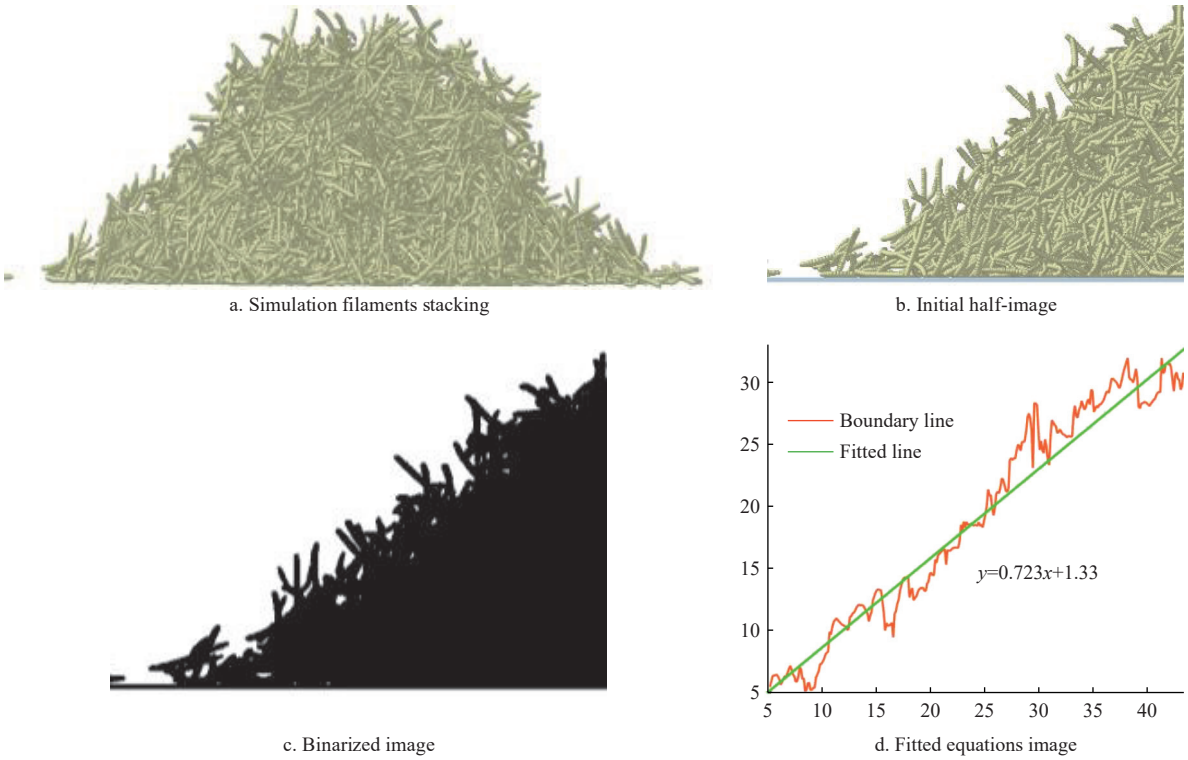

a. Simulation filaments stacking b. Initial half-image

c. Binarized image d. Fitted equations image

Figure 6 Simulation stack angle test of safflower filaments

2.2.3 Simulation model of safflower

The basic morphology of safflower is presented in Figure 7a. The discrete model of safflower consists of a fruit ball, necking, and filaments. The fruit ball has an ellipsoidal shape with a narrow top and wide bottom. Necking consists of dense clusters of filaments at the top of the fruit ball, and all filaments stem from the necking and grow in all directions. Therefore, necking reflects the main biomechanical characteristics of safflowers. A 3D model of safflower was created using SolidWorks 2022 based on the safflower characteristics and geometric parameters, as depicted in Table 1. The model consisted of a filament column. The filaments were drawn from the top of the fruiting bulb in an umbrella shape, and the filament clusters at the bottom were glued together to form necks (Figure 7b). The 3D model was saved in .igs format and imported into the EDEM software. Subsequently, a discrete element model of safflower was generated using the fast fill method, as shown in Figure 7c.

The bonding parameters directly reflect the magnitude of the simulated shear. Therefore, the safflower parameters were calibrated using simulated shear tests. The bonding parameters include the normal stiffness, shear stiffness, critical normal stress, critical shear stress, and bonded disk radius. By combining the

simulation parameters for the agricultural and floral materials, the obtained ranges for the bonding parameter values are presented in Table 3. After calibrating the contact parameters based on the physical shear test of safflower (Figure 8a), the virtual tool model was established (Figure 8b). The simulation shear tests were conducted with a speed of 20 mm/min and a shear distance of 35 mm.

a. Physical basic model b. 3D digital model c. Discrete element model

Figure 7 Simulation model of safflower

Table 3 Range of values for bonding parameters

Symbol	Simulation Parameter	Low level (–1)	High level (+1)
X_7	Normal stiffness per unit area of safflower/N·m^{-3}	1.00×10^8	1.00×10^{10}
X_8	Shear stiffness per unit area of safflower/N·m^{-3}	1.00×10^8	1.00×10^{10}
X_9	Critical normal Stress of safflower/MPa	1.00	100.00
X_{10}	Critical shear Stress of safflower/MPa	1.00	100.00
X_{11}	Bonded disk radius of safflower/mm	0.20	0.40

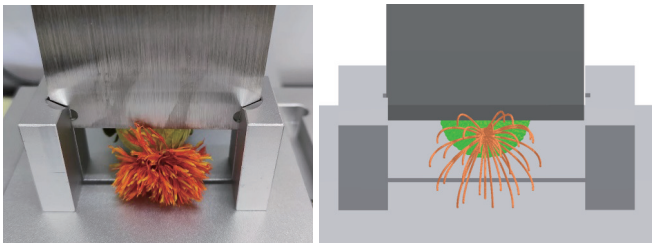

a. Physical shear model b. Simulation shear model

Figure 8 Safflower shear models

2.3 Design of parametric calibration tests

2.3.1 Design of calibration tests for contact parameters

Stacking angle tests of the simulated filaments were carried out based on filament particle models. Design-Expert 13 software applies a regular two-level factorial design to screen for significant factors. The characteristics were 6 factors with 2 levels for each factor. This is useful for estimating the main effects and interactions. Subsequently, the steepest climb test was conducted on the screened significant parameters to determine the region of proximity to the optimum value. The non-significant parameters were obtained at intermediate levels. The tests recorded the change in the relative error between the simulated and physical values of the stacking angle. Finally, the Box-Behnken design was carried out based on the relative error trend and optimum value region. The significance parameters were considered as high, medium, and low-level values to obtain the optimum contact parameter.

2.3.2 Design of calibration tests for bonding parameters

After establishing the safflower model and calibrating the contact parameters, a shear test simulation was conducted using the highest shear force as a response index. The test calibration process should ensure the reliability of the parameter ranges and avoid adverse effects caused by parameter values exceeding the ranges. According to the central composite design, combined with the upper and lower values of the parameters listed in Table 3, each numeric factor was set to 5 levels. Specifically, plus and minus alpha (axial points), plus and minus 1 (factorial points), the center points, and the bonding parameter code, as reported in Table 4.

Table 4 Parameter coding of the bonding model

Code	Parameter				
	X_7/N·m^{-3}	X_8/N·m^{-3}	X_9/MPa	X_{10}/MPa	X_{11}/mm
–2	1.00×10^8	1.00×10^8	1.00	1.00	0.20
–1	2.58×10^9	2.58×10^9	25.75	25.75	0.25
0	5.05×10^9	5.05×10^9	50.50	50.50	0.30
1	7.52×10^9	7.52×10^9	75.25	75.25	0.35
2	1.00×10^{10}	1.00×10^{10}	100.00	100.00	0.40

3 Results and discussion

3.1 Contact parameter calibration

3.1.1 Regular two-level factorial design test

The regular two-level factorial design can be implemented for screening through many factors to find the significant few. The contact parameters affecting the value of the filament stack angle included the safflower impact recovery coefficient (X_1), safflower-safflower rolling friction coefficient (X_2), safflower-safflower static friction coefficient (X_3), safflower-steel impact recovery coefficient (X_4), safflower-steel rolling friction coefficient (X_5), and safflower-steel static friction coefficient (X_6). The design of the tests and simulation results are listed in Table 5.

Table 5 Results of the regular two-level factorial design

Serial No.	X_1	X_2	X_3	X_4	X_5	X_6	θ_{cs}/(°)
1	0.25	0.15	0.15	0.60	0.40	0.60	24.90
2	0.05	0.15	0.15	0.10	0.10	0.30	23.50
3	0.25	0.60	0.6	0.10	0.10	0.60	59.90
4	0.05	0.60	0.15	0.60	0.10	0.60	44.00
5	0.25	0.60	0.15	0.60	0.10	0.30	46.47
6	0.25	0.60	0.15	0.10	0.40	0.30	32.84
7	0.05	0.15	0.15	0.60	0.40	0.30	21.46
8	0.25	0.15	0.15	0.10	0.10	0.60	28.50
9	0.25	0.15	0.6	0.60	0.10	0.30	41.13
10	0.05	0.15	0.6	0.10	0.40	0.60	33.55
11	0.25	0.60	0.6	0.60	0.40	0.60	38.57
12	0.05	0.60	0.15	0.10	0.40	0.60	45.00
13	0.05	0.60	0.6	0.60	0.40	0.30	51.73
14	0.25	0.15	0.6	0.10	0.40	0.30	23.20
15	0.05	0.15	0.6	0.60	0.10	0.60	35.20
16	0.05	0.60	0.6	0.10	0.10	0.30	59.66

Note: θ_{cs} denotes the value of the filament simulation stacking angle, (°).

The results of the regular two-level factorial design were analyzed using Design-Expert 13 software to obtain a Pareto chart, as shown in Figure 9. The significance of factor effects was determined using Bonferroni limits. Above the Bonferroni limit, the level of the factor was considered significant; below the Bonferroni limit, the level of the factor was considered insignificant[32]. The positive effects were defined as an increase in the stack angle as the level of the factor increased, while the negative effects were denoted as the opposite of the positive effects. The results ignored the effects of interactive factors and only considered the effects of individual factors. The effect of the stack angle was in the order of large to small: $X_3>X_2>X_6>X_1>X_5>X_4$, where the significant factors were X_2, X_3, and X_6. Among the three significant factors, X_2 and X_3

had positive effects, while X_6 had a negative effect. Consequently, the steepest climb test considered only these three factors as having significant effects. The non-significant factors X_1, X_4, and X_5 were taken as the median values of 0.15, 0.35, and 0.45, respectively.

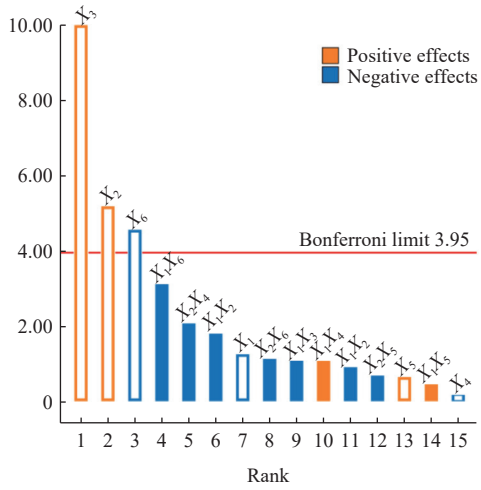

Figure 9 Pareto chart

3.1.2 Steepest climb test

The steepest climb test can be used to analyze the effect of factor levels on the evaluation indicators and further refine the range of factor levels[33]. The effects of X_2 and X_3 on the stacking angle were positive, while that of X_6 was negative. Therefore, the 10th group of data reported in Table 5 was the midpoint for the design, and the steepest climb test was conducted for contact parameters X_2, X_3, and X_6. The stacking angle and relative error were recorded for each test, and the results are listed in Table 6. The relative error equation is given by Equation (9).

$$R_c = \frac{|\theta_{ce} - \theta_{cs}|}{\theta_{ce}} \times 100\% \quad (9)$$

where, θ_{ce} is the physical average stack angle, (°); θ_{cs} is the simulated stack angle, (°); and R_c is the relative error between the physical and simulated stack angles.

Table 6 Results of the steepest climb test

Serial No. number	X_2	X_3	X_6	θ_{cs}/(°)	R_c/%
1	0.05	0.50	0.20	21.00	30.23
2	0.10	0.55	0.25	23.61	21.56
3	0.15	0.60	0.30	32.09	9.30
4	0.20	0.65	0.35	34.46	14.49
5	0.25	0.70	0.40	39.38	30.83

3.1.3 Box-Behnken test

According to the results obtained from the previous screening tests, the contact parameters that still needed to be calibrated were X_2, X_3, and X_6. The Box-Behnken designs were set up with five groups of center levels; in total, 17 groups of simulation tests were performed. The designs of the tests and the simulation results are listed in Table 7.

The analysis of variance (ANOVA) results for the quadratic regression model are presented in Table 8. The regression model (p<0.01) showed that the relationship between the quadratic regression equation obtained from the test and the stacking angle was very significant. The lack of fit term (p=0.47>0.05) was not significant compared to the pure error, and the fit was improved. The p-values of X_2, X_3, and X_3X_6 were less than 0.01, underlining a highly significant effect on the stacking angle. The p-values of X_6, X_2X_3, and X_2X_6 were less than 0.05, denoting a significant effect on the stacking angle. The significant factors were retained to establish a quadratic polynomial regression equation so that the accuracy of the response surface can be ensured, as depicted in Equation (10).

$$y_1 = -44.5 - 33.86X_2 + 481.66X_3 - 505.21X_6 - 86X_2X_3 + 315X_2X_6 + 685X_3X_6 + 49.6X_2^2 - 542.4X_3^2 + 84.6X_6^2 \quad (10)$$

Table 7 Designs and results of the Box-Behnken test

Serial No.	X_2	X_3	X_6	θ_{cs}/(°)	R_c/%
1	0.10	0.55	0.30	29.20	2.16%
2	0.20	0.60	0.35	35.01	0.13%
3	0.15	0.65	0.35	36.49	4.12%
4	0.15	0.60	0.30	31.97	0.02%
5	0.15	0.55	0.35	27.79	3.46%
6	0.20	0.65	0.30	34.01	1.23%
7	0.10	0.65	0.30	28.03	7.21%
8	0.20	0.55	0.30	30.04	4.98%
9	0.15	0.60	0.30	30.40	1.00%
10	0.15	0.65	0.25	28.60	0.20%
11	0.15	0.60	0.30	32.27	0.23%
12	0.15	0.60	0.30	30.47	9.67%
13	0.20	0.60	0.25	31.14	7.67%
14	0.15	0.60	0.30	30.15	6.21%
15	0.10	0.60	0.25	31.34	7.94%
16	0.10	0.60	0.35	30.06	9.67%
17	0.15	0.55	0.25	30.75	12.96%

Table 8 ANOVA results for contact parameters

Source of variation	Mean square	Degree of freedom	Quadratic Sum	*p-value*	Significance
Model	82.41	9	9.16	<0.01	**
X_2	16.73	1	16.73	<0.01	**
X_3	10.93	1	10.93	<0.01	**
X_6	7.07	1	7.07	0.03	*
X_2X_3	6.60	1	6.60	0.04	*
X_2X_6	6.63	1	6.63	0.04	*
X_3X_6	29.43	1	29.43	<0.01	**
X_2^2	0.064	1	0.06	0.80	
X_3^2	3.09	1	3.09	0.12	
X_6^2	2.13	1	2.13	0.18	
Residual	6.88	7	0.98		
Lack of fit	2.98	3	0.99	0.47	
Pure error	3.90	4	0.98		
Total	89.29	16			

Note: *indicates significant (0.01<p<0.05), **indicates very significant (p<0.01).

3.1.4 Analysis of contact parameter response curves

According to the regression model described in Equation (10), the response surface of the contact parameters was established, as shown in Figure 10. The steepness of the response surface reflects the influence degree of the interaction terms on the response values; the steeper the surface is, the more significant the influence of the interaction terms on the response values becomes[34].

As shown in Figure 10a, the stacking angle increased and then decreased with the filament-filament static friction coefficient X_3. Furthermore, the filament-filament kinetic friction coefficient X_2 increased with increasing values. The steepness of X_2 was greater than that of X_3. This proved that increasing the value of X_2 increased the stack angle; accordingly, X_2 was significantly greater than X_3.

As shown in Figure 10b, the stacking angle decreases with an increase in the filament-steel static friction coefficient X_6. However, with a simultaneous increase in the filament-filament kinetic friction coefficient X_2 and filament-steel static friction coefficient X_6, the stacking angle kept increasing, indicating that the filament-filament kinetic friction coefficient X_2 was significantly larger than the filament-steel static friction coefficient X_6. As shown in Figure 10c, the stacking angle decreased with an increase in the filament-steel static friction coefficient X_6, while the filament-filament static friction coefficient X_3 showed a tendency to first increase and then decrease. In summary, the order of influence of the three parameters was $X_2 > X_3 > X_6$.

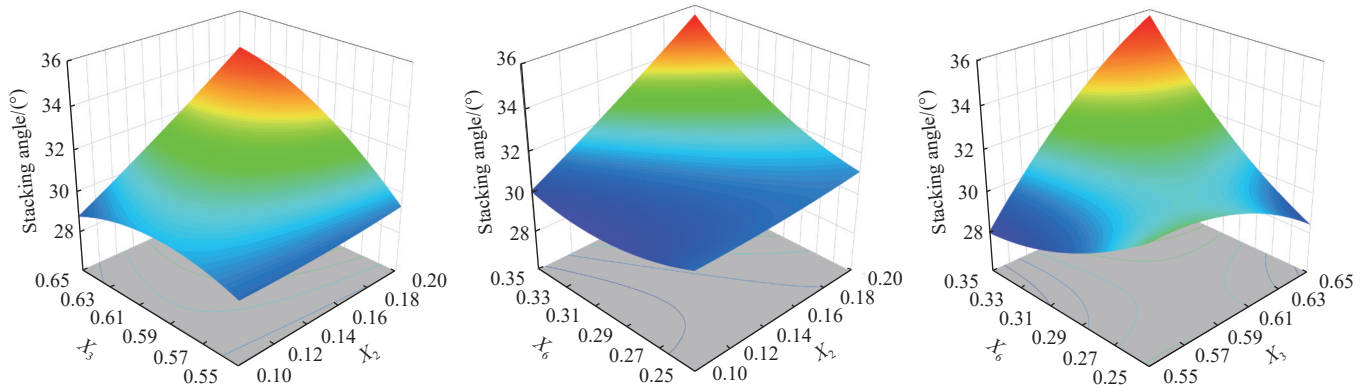

a. Effects of X_2 and X_3 b. Effects of X_2 and X_6 c. Effects of X_3 and X_6

Figure 10 Effect of interaction terms on stacking angle

The optimization module of the Design-Expert software was used to solve Equation (10) and optimize the regression model and simulation parameters, setting the physical test value of the stacking angle (30.08°) as the target value. The corresponding objective and constraint equations are presented as follows:

$$\begin{cases} \text{target value} = 30.08^\circ \\ \text{s.t.} \begin{cases} 0.19 \le X_2 \le 0.21 \\ 0.56 \le X_3 \le 0.58 \\ 0.30 \le X_6 \le 0.32 \end{cases} \end{cases} \tag{11}$$

Based on the Design-Expert constraint-solving tool presented in Equation (11), the errors of the minimum extreme points X_2, X_3, and X_6 were determined as 0.20, 0.57, and 0.31, respectively. The solved quadratic regression equation for the parameters yielded a fitted value of 31.09° for the stacking angle in the simulation tests. According to the physical tests, the average stacking angle was measured as 30.8°. Therefore, the relative error between the simulated and physical values of the stacking angle was 3.19%, which indicated that the basic contact parameters of filament particles were feasible.

3.2 Bonding parameter calibration

3.2.1 Central composite design test

Based on the calibrated contact parameters of safflower, shear simulation tests were conducted based on a central composite design. The bonding parameter values of normal stiffness X_7, shear stiffness X_8, critical normal stress X_9, critical shear stress X_{10}, and bonded disk radius X_{11} were determined during the tests. In total, 27 groups of simulation tests were conducted, and the corresponding central composite design results are listed in Table 9.

As shown in Table 10, the regression model had a P-value <0.0006 (p<0.01). This indicated that the model was highly significant regarding the relationship between the three factors, namely, the normal contact stiffness X_7, shear contact stiffness X_8, and bond radius X_{11}, and shear force F_c. The model coefficient of determination (R^2) was 0.9854. Therefore, the model can be used to solve the bond parameters optimally. Four terms in the model, namely, X_7, X_8, X_{11}, and interaction term X_7X_8 (p<0.01), had highly significant effects on F_c. Four other terms (p<0.05), namely, the interaction terms X_7X_{11}, X_8X_{11}, X_7^2, and X_8^2, had significant effects on F_c whereas the rest of the terms were not significant.

Table 9 Results of the central composite design

Serial number	X_7/N·m^{-3}	X_8/N·m^{-3}	X_9/MPa	X_{10}/MPa	X_{11}/mm	F_{cs}/N
1	5.05×10^9	5.05×10^9	50.50	50.50	0.20	21.20
2	1.00×10^{10}	5.05×10^9	50.50	50.50	0.30	56.12
3	5.05×10^9	1.00×10^{10}	50.50	50.50	0.30	52.30
4	5.05×10^9	5.05×10^9	50.50	1.00	0.30	34.21
5	7.53×10^9	7.52×10^9	25.75	25.75	0.35	68.70
6	5.05×10^9	5.05×10^9	100.00	50.50	0.30	35.00
7	2.58×10^9	2.58×10^9	25.75	75.25	0.25	8.17
8	2.58×10^9	7.52×10^9	25.75	75.25	0.35	49.40
9	7.52×10^9	7.52×10^9	75.25	25.75	0.25	40.90
10	5.05×10^9	1.00×10^8	50.50	50.50	0.30	14.42
11	7.53×10^9	2.58×10^9	75.25	75.25	0.25	25.70
12	2.58×10^9	2.58×10^9	75.25	25.75	0.25	18.05
13	2.58×10^9	2.58×10^9	25.75	25.75	0.35	35.60
14	1.00×10^8	5.05×10^9	50.50	50.50	0.30	14.25
15	5.05×10^9	5.05×10^9	1.00	50.50	0.30	40.60
16	5.05×10^9	5.05×10^9	50.50	50.50	0.40	75.30
17	2.58×10^9	7.52×10^9	75.25	25.75	0.35	48.30
18	2.58×10^9	2.58×10^9	75.25	75.25	0.35	35.70
19	2.58×10^9	7.52×10^9	75.25	75.25	0.25	18.90
20	7.52×10^9	7.52×10^9	75.25	75.25	0.35	75.30
21	2.58×10^9	7.52×10^9	25.75	25.75	0.25	21.30
22	7.52×10^9	2.58×10^9	25.75	75.25	0.35	32.20
23	5.05×10^9	5.05×10^9	50.50	100.00	0.30	39.90
24	7.52×10^9	2.58×10^9	25.75	25.75	0.25	29.07
25	7.52×10^9	2.58×10^9	75.25	25.75	0.35	32.84
26	5.05×10^9	5.05×10^9	50.50	50.50	0.30	48.60
27	7.52×10^9	7.52×10^9	25.75	75.25	0.25	57.60

A quadratic regression model of safflower and its influencing factors under the action of shear was established by a fitting analysis conducted on the central composite design. Considering that there were more variance-influencing factors, considering that the model was significant and the lack-of-fit term was not significant, the non-significant term was excluded. Accordingly, the

second-order regression model was optimized and adjusted to obtain the regression equation, as shown in Equation (12).

Table 10 ANOVA results for bonding parameters

Source of variation	Mean square	Degree of freedom	Quadratic sum	*p*-value	Significance
Model	8542.18	20	427.11	<0.01	**
X_7	1848.54	1	1848.54	<0.01	**
X_8	2376.66	1	2376.66	<0.01	**
X_9	12.83	1	12.83	0.46	
X_{10}	15.99	1	15.99	0.42	
X_{11}	2960.37	1	2960.37	<0.01	**
X_7X_8	423.43	1	423.43	<0.01	**
X_7X_9	23.30	1	23.30	0.33	
X_7X_{10}	57.65	1	57.65	0.15	
X_7X_{11}	136.95	1	136.95	0.04	*
X_8X_9	27.17	1	27.17	0.30	
X_8X_{10}	80.06	1	80.06	0.10	
X_8X_{11}	141.91	1	141.91	0.04	*
X_9X_{10}	32.52	1	32.52	0.26	
X_9X_{11}	22.16	1	22.16	0.34	
$X_{10}X_{11}$	2.33	1	2.33	0.75	
X_7^2	127.41	1	127.41	0.05	*
X_8^2	171.94	1	171.94	0.03	*
X_9^2	75.21	1	75.21	0.11	
X_{10}^2	88.69	1	88.69	0.09	
X_{11}^2	3.16	1	3.16	0.71	
Residual	126.14	6	21.02		
Cor Total	8668.32	26			

$$y_2 = -32.224 + 1.048X_7 \times 10^{-8} - 2.805X_8 \times 10^{-9} + 49.723X_{11} + 8.398 \times 10^{-19}X_7X_8 - 2.364 \times 10^{-8}X_7X_{11} + 2.407 \times 10^{-8}X_8X_{11} - 4.607 \times 10^{-19}X_7^2 - 5.351 \times 10^{-19}X_8^2 \quad (12)$$

3.2.2 Analysis of bonding parameter response curves

According to the regression model in Equation (12), the response surfaces of the reaction normal contact stiffness interacted with the shear contact stiffness term X_7X_8, the normal contact stiffness interacted with the bond radius term X_7X_{11}, and the shear contact stiffness interacted with the bond radius term X_8X_{11} to the shear force. As shown in Figure 11a, the shear force increased with the normal contact stiffness X_7 and shear contact stiffness X_8, and the shear contact stiffness X_8 was steeper than the normal contact stiffness X_7. This indicates that increasing both the normal and shear stiffnesses of the safflower model increased the shear force, and the shear contact stiffness X_8 was significantly larger than the normal contact stiffness X_7. As shown in Figure 11b, the shear force also increases with the increase of the bond bonding key radius X_{11}, especially at 0.2-0.3 mm the response surface changes were larger. This indicates that the safflower particle bond radius increases, and the formation of bonds increases the shear force further when the normal contact stiffness, X_7, is unchanged. As shown in Figure 11c, the observed trend was similar to that shown in Figure 11b; however, the steepness of the response surface was higher. The results showed that the significance of bond radius X_{11} was greater than that of normal contact stiffness X_7. Considering these three parameters together, the order of influence of the shear force was $X_{11}>X_8>X_7$.

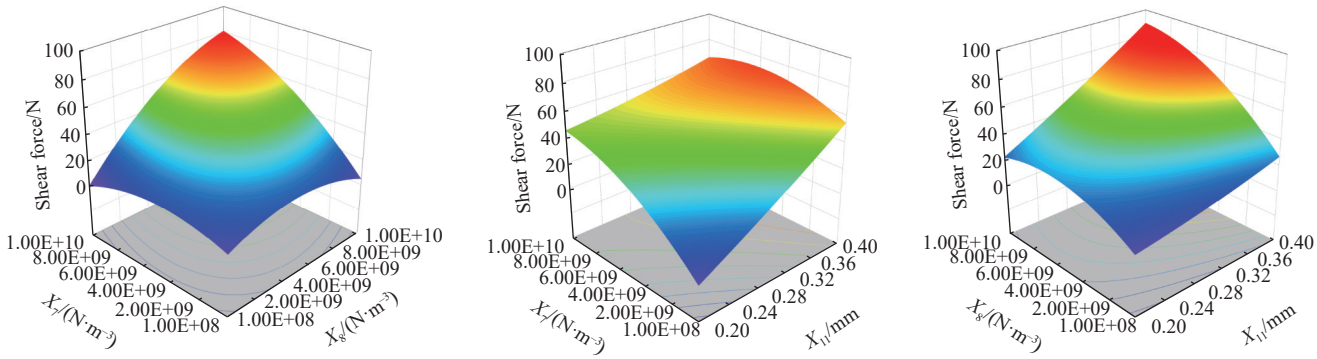

a. Effects of X_7 and X_8 b. Effects of X_7 and X_{11} c. Effects of X_8 and X_{11}

Figure 11 Effects of interaction terms on the most shear force

In the regression Equation (12), the critical normal stress X_9 and critical shear stress X_{10} were not significant enough, so their intermediate values of 50.50 MPa, and 50.50 MPa, respectively. The optimization module of the Design-Expert software was used to solve Equation (12), setting the physical test value of the shear force (43.36 N) as the target value. The corresponding objective and constraint equations are presented as follows:

$$\begin{cases} \text{target value} = 43.36\ \text{N} \\ \text{s.t.} \begin{cases} 3.56 \times 10^9 \le X_7 \le 7.39 \times 10^9 \\ 2.86 \times 10^9 \le X_8 \le 6.77 \times 10^9 \\ 0.28 \le X_{11} \le 0.32 \end{cases} \end{cases} \quad (13)$$

Regarding the optimal solution of Equation (13), the normal contact stiffness X_7, shear contact stiffness X_8, and bond radius X_{11} were 5.48×10^9 N/m^3, 4.82×10^9 N/m^3, and 0.30 mm, respectively.

3.2.3 Optimal parameter combination determination and model validation

To verify the accuracy of the contact and bonding parameters, the general generalizability of the discrete element model developed for safflower simulation was implemented. After calibrating the optimal combination of safflower contact and bonding parameters, the accuracy of the model was verified using physical and simulated shear tests. The highest shear was used as the response index, and the other setup conditions were kept unchanged, as listed in Table 11.

In the physical test, the maximum shear force (F_c) was 58.27 N, and the average physical shear force (F_{ce}) was 43.36 N. In the simulation test, the maximum shear force (F_s) was 54.60 N, and the average simulation shear force (F_{se}) was 39.92 N. The relative error (R_f) between the physical and simulation tests was 5.29 %, which indicated that the calibrated safflower simulation parameters were

accurate.

The change in resistance during the safflower shear test is shown in Figure 12a. In the compression stage, the change in the shear force was small with an increase in displacement. The main reason for this may be that the safflower necking had some elastic capacity and underwent compression. In the shear stage, the force increased sharply with an increase in displacement, and the safflower reached the maximum shear force *Fs* when the load exceeded its shear strength. In the fracture stage, the shear force acting on the remaining part of the sample decreased gradually with a continuous increase in displacement until the end of the test. As shown in Figure 12b, the simulation curve was highly consistent with the changing trend of the physical test curve. This implies that the established safflower simulation model can reflect the change rule of force with displacement in the shear process. In summary, the calibrated model of safflower accurately reflected its shear mechanical properties, indicating that the established safflower model was accurate.

Table 11 Safflower discrete element simulation parameters

Type	Parameter	Value
Contact parameters	Impact recovery coefficient of safflower-safflower	0.15
	Rolling friction coefficient of safflower-safflower	0.57
	Static friction coefficient of safflower-safflower	0.20
	Impact recovery coefficient of safflower-steel	0.35
	Rolling friction coefficient of safflower-steel static	0.31
	friction coefficient of safflower-steel	0.45
Bonding parameters	Normal stiffness per unit area of safflower/(N·m^{-3})	5.48×10^{9}
	Shear stiffness per unit area of safflower/(N·m^{-3})	4.82×10^{9}
	Critical normal Stress of safflower/MPa	50.50
	Critical shear Stress of safflower/MPa	50.50
	Bonded disk radius of safflower/mm	0.30

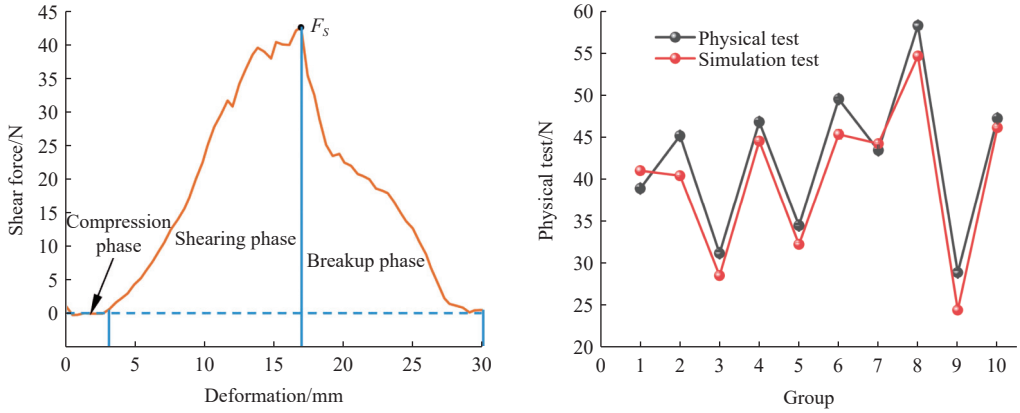

a. Shear force versus displacement

b. Comparison of physical and simulation curves

Figure 12 Physical shear test and model validation

4 Conclusions

Safflower is a flexible crop that lacks a basis for relevant actuator parameters and suffers from severe damage during harvest. A possible solution to this problem is using discrete-element simulations to study the microscopic mechanisms of safflowers. A combination of physical and simulation tests was used to establish a discrete element model of safflower in this study. Accordingly, the following conclusions are drawn.

(1) From regular two-level factorial design results, the safflower-safflower kinetic friction coefficient X_2, safflower-safflower static friction coefficient X_3, and safflower-steel static friction coefficient X_6 had a significant effect on the stacking angle of safflower. Other simulation parameters have no significant effect on it.

(2) The contact parameters between safflower and steel were determined by filament stacking angle test. From the steepest climb and the Box-Behnken test result, X_1, X_2, X_3, X_4, X_5, and X_6 values were 0.15, 0.20, 0.57, 0.35, 0.25, and 0.31, respectively. The relative error with the measured value of physical realization was 3.19%, which indicated that the contact parameters of safflower were feasible.

(3) The results of the central composite design showed the established quadratic regression model of the most shear force has good reliability and accuracy. The normal contact stiffness X_7, shear contact stiffness X_8, and bond radius X_{11} were significant model terms regarding the most shear force. From the solution of optimization combination, the normal contact stiffness X_7, shear contact stiffness X_8, critical normal stress X_9, critical shear stress X_{10}, and bond radius X_{11} were 5.48×10^9 N/m^3, 4.82×10^9 N/m^3, 50.50 MPa, 50.50 MPa, and 0.3 mm, respectively.

(4) The results of the validation test of safflower physical shear under the optimal parameter combination show the average relative error between the simulated and the shear force was 5.29 %, indicating the errors are small. In addition, the simulation curves were compared with the physical test curves, and the change trends of the two curves were highly consistent. Therefore, the reliability and accuracy of the discrete element model and simulation parameters of safflower are verified.

This study provides theoretical support for the harvesting process of safflowers and the design of relevant key components. It is also helpful for the modeling and biomechanical characterization of other similar crops. In establishing the discrete element model of safflower, further studies are needed to investigate the interference factors, such as different filament morphologies and actual bast and floral stem composition of safflower necking.

Acknowledgements

This study was supported by the National Natural Science Foundation of China (Grant Nos. 52265041 and 31901417), and also acknowledges the assistance provided by the Xinjiang Key Laboratory of Intelligent Agricultural Equipment.

[References]

[1] De Oliveira Neto S S, Zeffa D M, Freiria G H, Zoz T, Da Silva C J,

Zanotto M D, et al. Adaptability and stability of safflower genotypes for oil production. Plants, 2022; 11(5): 708.

[2] Zhang Z G, Shi R M, Xing Z Y, Guo Q F, Zeng C. Improved faster region based convolutional neural networks (R-CNN) model based on split attention for the detection of safflower filaments in natural environments. Agronomy, 2023; 13(10): 2596.

[3] Hu Z, Zeng H, Ge Y, Wang W, Wang J. Simulation and experiment of gas-solid flow in a safflower sorting device based on the CFD-DEM coupling method. Processes, 2021; 9(7): 1239.

[4] Zhang Z G, Xing Z Y, Zhao M Y, Yang S P, Guo Q F, Shi R W, et al. Detecting safflower filaments using an improved YOLOv3 under complex environments. Transactions of the CSAE, 2023; 39(3): 162–170. (in Chinese)

[5] Wang X R, Xu Y, Zhou J P, Chen J R. Safflower picking recognition in complex environments based on an improved YOLOv7. Transactions of the CSAE, 2023; 39(6): 169–176. (in Chinese)

[6] Cao W B, Lian D G, Niu C, An L L, Yang S P, Chen B B. Harvest performance test and parameter optimization of comb-type safflower-filaments picking head at same height. Transactions of the CSAE, 2018; 34(22): 36–44. (in Chinese)

[7] Azimi S, Chegini G, Kianmehr M H. Design and manufacture of safflower petal harvester machine. Mechanics & Industry, 2012; 13(5): 301–305.

[8] Chen F, Ge Y, Zhang L, Qi Z H, Zeng H F. Design and experiment of the strip-collected pre-positioning mechanism for saf-flower picking robots. Transactions of the CSAE, 2021; 37(15): 10–19. (in Chinese)

[9] Zhang Z G, Zhao M Y, Xing Z Y, Liu X F. Design and test of double-acting opposite direction cutting end effector for safflower harvester. Transactions of the CSAM, 2022; 53(12): 160–170. (in Chinese)

[10] Zhang S L, Zhao H B, Wang X Z, Dong J X, Zhao P F, Yang F F, et al. Discrete element modeling and shear properties of the maize stubble-soil complex. Computers and Electronics in Agriculture, 2023; 204: 107519.

[11] Li X Y, Du Y F, Mao E R, Zhang Y A, Liu L, Guo D F. Design and experiment of corn low damage threshing device based on DEM. Int J Agric & Biol Eng, 2023; 16(3): 55–63.

[12] Zhang Z Y, Mei F W, Xiao P J, Zhao W, Zhu X H. Discrete element modelling and simulation parameters calibration for the compacted straw cube. Biosystems Engineering, 2023; 230: 301–312.

[13] Huang Y X, Wang B T, Yao Y X, Ding S P, Zhang J C, Zhu R X. Parameter optimization of fluted-roller meter using discrete element method. Int J Agric & Biol Eng, 2018; 11(6): 65–72.

[14] Shi L R, Zhao W Y, Sun B G, Sun W, Zhou G. Determination and analysis of basic physical and contact mechanics parameters of quinoa seeds by DEM. Int J Agric & Biol Eng, 2023; 16(5): 35–43.

[15] Horabik J, Molenda M. Parameters and contact models for DEM simulations of agricultural granular materials: A review. Biosystems Engineering, 2016; 147: 206–225.

[16] Zhao H B, Huang Y X, Liu Z D, Liu W Z, Zheng Z Q. Applications of discrete element method in the research of agricultural machinery: A review. Agriculture, 2021; 11(5): 425.

[17] Ahmad M R, Chen B, Haque M A, Shah S F A. Development of a sustainable and innovant hygrothermal bio-composite featuring the enhanced mechanical properties. Journal of Cleaner Production, 2019; 229: 128–143.

[18] Leblicq T, Smeets B, Ramon H, Saeys W. A discrete element approach for modelling the compression of crop stems. Computers and Electronics in Agriculture, 2016; 123: 80–88.

[19] Ma Z, Traore S N, Zhu Y, Li Y M, Xu L Z, Lu E, et al. DEM simulations and experiments investigating of grain tank discharge of a rice combine harvester. Computers and Electronics in Agriculture, 2022; 198: 107060.

[20] Peng F, Huang Z, Fang F. Modeling and experiments of chewing mechanical properties of pellet feed using discrete element method. Int J Agric & Biol Eng, 2020; 13(4): 37–44.

[21] Chen T, Yi S J, Tao G X, Qu S M, Li R. Establishment of discrete element model and parameter calibration of alfalfa stem in budding stage. Transactions of the CSAM, 2023; 54(5). (in Chinese)

[22] Zhou J, Sun W T, Liang Z A. Construction of discrete element flexible model for jerusalem artichoke root-tuber at harvest stage. Transactions of the CSAM, 2023; 54(10): 124–132. (in Chinese)

[23] Li X, Du Y, Liu L, Zhang Y A, Guo D F. Parameter calibration of corncob based on DEM. Advanced Powder Technology, 2022; 33(8): 103699.

[24] Zhang Z G, Xu H W, Xue H T, Ni C, Wang C. Calibration and experiment of discrete element parameters of panax notoginseng stem. Transactions of the CSAM, 2023; 54(11): 61–70, 91. (in Chinese)

[25] Xing Z Y, Zhang Z G, Shi R M, Guo Q F, Zeng C. Filament-necking localization method via combining improved PSO with rotated rectangle algorithm for safflower-picking robots. Computers and Electronics in Agriculture, 2023; 215: 108464.

[26] Zhao L, Zhou H P, Xu L Y, Song S Y, Zhang C, Yu Q X. Parameter calibration of coconut bran substrate simulation model based on discrete element and response surface methodology. Powder Technology, 2022; 395: 183–194.

[27] Shi G K, Li J B, Ding L P, Zhang Z Y, Ding H Z, Li N, et al. Calibration and tests for the discrete element simulation parameters of fallen jujube fruit. Agriculture, 2021; 12(1): 38.

[28] Mudarisov S, Farkhutdinov I, Khamaletdinov R, Khasanov E, Mukhametdinov A. Evaluation of the significance of the contact model particle parameters in the modelling of wet soils by the discrete element method. Soil and Tillage Research, 2022; 215: 105228.

[29] Jiménez-Herrera N, Barrios G K P, Tavares L M. Comparison of breakage models in DEM in simulating impact on particle beds. Advanced Powder Technology, 2018; 29(3): 692–706.

[30] Liu F, Zhang J, Chen J. Modeling of flexible wheat straw by discrete element method and its parameter calibration. Int J Agric & Biol Eng, 2018; 11(3): 42–46.

[31] Zhao W, Chen M, Xie J, Cao S L, Wu A B, Wang Z W. Discrete element modeling and physical experiment research on the biomechanical properties of cotton stalk. Computers and Electronics in Agriculture, 2023; 204: 107502.

[32] Wu Z Y, Wang X S, Liu D W, Xie F P, Ashwehmbom L G, Zhang Z Z, et al. Calibration of discrete element parameters and experimental verification for modelling subsurface soils. Biosystems Engineering, 2021; 212: 215–227.

[33] Guo J, Karkee M, Yang Z, Fu H, Li J, Jiang Y L, et al. Discrete element modeling and physical experiment research on the biomechanical properties of banana bunch stalk for postharvest machine development. Computers and Electronics in Agriculture, 2021; 188: 106308.

[34] Golzarijalal M, Ong L, Harvie D J E, Gras S L. Experimental investigation, numerical simulation and RSM modelling of the freezing and thawing of Mozzarella cheese. Food and Bioproducts Processing, 2024; 143: 143–157.